

# Red Sequence Cluster Finding in the Millennium Simulation

J.D. Cohn<sup>1</sup>, A.E. Evrard<sup>2</sup>, M. White<sup>3,4</sup>, D. Croton<sup>4</sup>, E. Ellingson<sup>5</sup>

<sup>1</sup>*Space Sciences Laboratory, Univ. of California, Berkeley*

<sup>2</sup>*Departments of Physics and Astronomy and MCTP, Univ. of Michigan*

<sup>3</sup>*Department of Physics, Univ. of California, Berkeley*

<sup>4</sup>*Department of Astronomy, Univ. of California, Berkeley*

<sup>5</sup>*Department of Astrophysical and Planetary Sciences, Center for Astrophysics & Space Astronomy (CASA), Univ. of Colorado*

1 November 2018

## ABSTRACT

We investigate halo mass selection properties of red-sequence cluster finders using galaxy populations of the Millennium Simulation (MS). A clear red sequence exists for MS galaxies in massive halos at redshifts  $z < 1$ , and we use this knowledge to inform a cluster-finding algorithm applied to  $500 h^{-1}$  Mpc projections of the simulated volume. At low redshift ( $z = 0.4$ ), we find that 90% of the clusters found have galaxy membership dominated by a single, real-space halo, and that 10% are blended systems for which no single halo contributes a majority of a cluster’s membership. At  $z = 1$ , the fraction of blends increases to 22%, as weaker redshift evolution in observed color extends the comoving length probed by a fixed range of color. Other factors contributing to the increased blending at high- $z$  include broadening of the red sequence and confusion from a larger number of intermediate mass halos hosting bright red galaxies of magnitude similar to those in higher mass halos. Our method produces catalogs of cluster candidates whose halo mass selection function,  $p(M|N_{\text{gal}}, z)$ , is characterized by a bimodal log-normal model with a dominant component that reproduces well the real-space distribution, and a redshift-dependent tail that is broader and displaced by a factor  $\sim 2$  lower in mass. We discuss implications for X-ray properties of optically selected clusters and offer ideas for improving both mock catalogs and cluster-finding in future surveys.

**Key words:** cosmology: clusters of galaxies, large scale structure

## 1 INTRODUCTION

The abundance and distribution of massive dark matter halos provide a sensitive probe of cosmology and theories of structure formation. The galaxies within these halos also have their evolution strongly affected by their hosts. Clusters of galaxies are the observational realization of such halos which has inspired multi-wavelength campaigns to find and characterize them. With the advent of large format CCD cameras on large telescopes, which can identify galaxies to high redshifts over wide fields, there has been renewed interest in optical searches for clusters using multicolor imaging (Kaiser et al 1998; Lubin et al 2000; Gladders & Yee 2000, 2005; Gladders et al 2006; Miller et al 2005; Koester et al 2007), see Gal (2006) for a review of optical cluster finding methods. In particular, methods which identify the cluster red sequence (Bower, Lucey, & Ellis 1992; Lopez-Cruz 1997; Gladders & Yee 2000; Lopez-Cruz, Barkhouse & Yee 2004; Gal, Lubin & Squires 2005; Gladders & Yee 2005; Gladders et al 2006; Wilson et al 2006) have attained sig-

nificant success in identifying cluster candidates over wide fields to  $z \simeq 1$  and above.

Because red sequence galaxies dominate the cluster population, including the reddest galaxies at a given redshift and becoming redder with increasing redshift, the restriction to red sequence colors approximately isolates a redshift slice. This redshift filtering increases the signal-to-noise of cluster detection by largely eliminating projection effects from unassociated structures along the line of sight. However, contamination is still expected from blue galaxies at even higher redshift than the cluster and from galaxies near enough to the cluster to lie within the narrow, red-sequence color region. This residual contamination is the focus of this work.

We are motivated by current red sequence based cluster searches, such as the SDSS (Koester et al 2007; Miller et al 2005), in particular by those using two filters only such as the RCS and the RCS-2 (Gladders & Yee 2000; Gladders et al

2006) and SpARCS (Wilson et al 2006)<sup>1</sup>. We investigate the nature of the cluster population selected by a two filter method applied to mock galaxy samples of the Millennium Simulation (MS) (Springel et al 2005; Croton et al 2006; Lemson et al 2006; Kitzbichler and White 2007). Throughout this paper, we use “clusters” to refer to objects found by the algorithm and “halos” to refer to the dark matter halos identified in the simulation using the full 3D dark matter distribution. We use joint halo–cluster membership — identifying the MS halos to which each cluster’s galaxies belong — to categorize the purity and completeness of the cluster population. (Joint halo–cluster membership is defined by taking a cluster, found using the red sequence method below, and then identifying the MS halos to which its galaxies belong.) Our cluster finder is patterned after the scheme used in three dimensions to identify halos. We apply a circular overdensity algorithm, centered on bright  $z$ -band galaxies, to spatial projections of the galaxy populations at the discrete redshifts  $z = 0.41, 0.69$  and  $0.99$ .

An advantage of the Millennium Simulation is that it provides mock clusters situated in their correct cosmological context as part of the evolving cosmic web. Including the cosmic web is significant because projections of superclusters, structures that tend to align along filaments meeting at the cluster of interest, provide a major source of confusion for cluster identification that is difficult to otherwise model. By having available the full 3D galaxy and dark matter distribution in the simulation we are able to monitor and isolate different physical effects which can influence red sequence cluster finding.

The outline of the paper is as follows. We describe our methods in §2 and give our findings for the MS in §3. We consider some implications and properties of the blends in §4 and discuss properties causing and correlating with the blending which might extend beyond our particular search algorithm and simulation in §5. We conclude in §6. The appendix compares different purity and completeness definitions in use.

## 2 METHODS

The context for our study is the model of the spatial distribution of massive halos and the galaxies that inhabit them provided by the Millennium simulation (Springel et al 2005; Lemson et al 2006). This is a collisionless dark matter simulation performed in a periodic cube  $500 h^{-1} \text{Mpc}$  (comoving) on a side, using  $10^{10}$  particles for a cosmology with parameters  $(\Omega_m, \Omega_\Lambda, \sigma_8, \Omega_b, h, n) = (0.25, 0.75, 0.9, 0.045, 0.73, 1.0)$ . Mock galaxies, with luminosities and colors, are generated by post-processing the dark matter halo merger trees with a semi-analytic prescription for the gas dynamics and feedback. For details, see Croton et al (2006); Kitzbichler and White (2007). In particular, our version is that described in detail in Croton et al (2006), however with the updated dust prescription of Kitzbichler and White (2007) which better models dust extinction at higher redshifts.

<sup>1</sup> For up to date information about the RCS and SpARCS surveys see <http://www.astro.utoronto.ca/~gladders/RCS/> and <http://spider.ipac.caltech.edu/staff/gillian/SpARCS>.

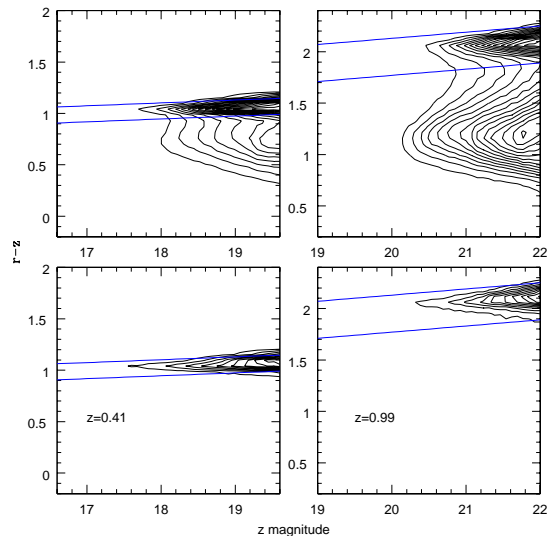


**Figure 1.** Distributions of  $r-z$  colors and magnitudes at  $z = 0.41$  (left) and  $0.99$  (right) for all  $z$ -band magnitude-limited galaxies (top) and for those galaxies in halos with at least eight members (bottom). Contours are in steps of  $\sim 770$  (left, top),  $\sim 260$  (left, bottom),  $\sim 360$  (right, top) and  $\sim 60$  (right, bottom) galaxies. Straight lines show the color–magnitude region defining the red sequence at each redshift.

We focus our cluster finding investigation on local confusion, projections on spatial scales  $\lesssim 250 h^{-1} \text{Mpc}$  of a target halo that will, at these redshifts, be barely resolved by photometric redshifts of the next-generation surveys (DES<sup>2</sup>, CFHT-LS<sup>3</sup>, Pan-Starrs<sup>4</sup>, KIDS<sup>5</sup>, SNAP<sup>6</sup>, LSST<sup>7</sup>). (Although the scales these surveys might resolve are comparable to the box size considered here, these surveys are not necessarily using only the RS method described in this paper.) We use the simulated galaxy and halo catalogues at three fixed epochs given by redshifts  $z = 0.41, 0.69$  and  $0.99$ . These values span much of the expected redshift range of interest for a survey such as the RCS. Halos in the simulation are found by using a friends-of-friends algorithm (Davis et al. 1985) and galaxy membership is determined based on this. The friends-of-friends linking length (0.2 times the mean inter-particle spacing) can link objects into one large halo which by eye look to be smaller components, we note below where our results show signs of this effect. Halo masses are given in terms of  $M_{200c}$  (denoted as  $M$  henceforth), the mass enclosed within a radius interior to which the mean density is 200 times the critical density at that epoch. At our redshifts there were 1268, 805 and 426 halos with  $M \geq 10^{14} h^{-1} M_\odot$  and 113, 47 and 19 halos with  $M \geq 3 \times 10^{14} h^{-1} M_\odot$ .

For the red sequence search, the SDSS  $r$  and  $z$  filters, which bracket the 4000 Angstrom break for approximately  $0.5 \leq z \leq 1$ , are employed. At the highest redshift, we also

<sup>2</sup> <http://www.darkenergysurvey.org>

<sup>3</sup> <http://cadwww.hia.nrc.ca/cfht/cfhtls/>

<sup>4</sup> <http://pan-starrs.ifa.hawaii.edu>

<sup>5</sup> <http://www.astro.wise.org/projects/KIDS/>

<sup>6</sup> <http://snap.lbl.gov>

<sup>7</sup> <http://www.lsst.org>

**Table 1.** Changes in redshifts, colors and cuts for three boxes used.

Redshift	$z_{\min}$	$z_{\max}$	intercept	slope	max RS dist. $\Delta_{\perp}$	$\frac{d(r-z)}{d(h^{-1}\text{Gpc})}$ low/high	$\frac{dz-\text{mag}}{d(h^{-1}\text{Gpc})}$ low/high
0.41	0.31	0.51	0.52	0.028	0.078	-0.72/ 1.30	-0.56/0.52
0.69	0.57	0.81	0.72	0.052	0.14	-1.10/0.36	-0.80/0.64
0.99	0.85	1.14	0.75	0.060	0.18	-0.40/0.72	-1.08/1.40

Change in redshift across the Millennium box at different redshifts, red sequence intercept and slope, maximum distance from red sequence in color-magnitude space ( $\Delta_{\perp}$ ), the  $r-z$  color change across the box (to front, and then to back, per  $h^{-1}$  Gpc), and the  $z$  magnitude change across the box. Color and magnitude changes are taken from the Bruzual-Charlot (2003) model as described in the text, see also Fig. 2a.

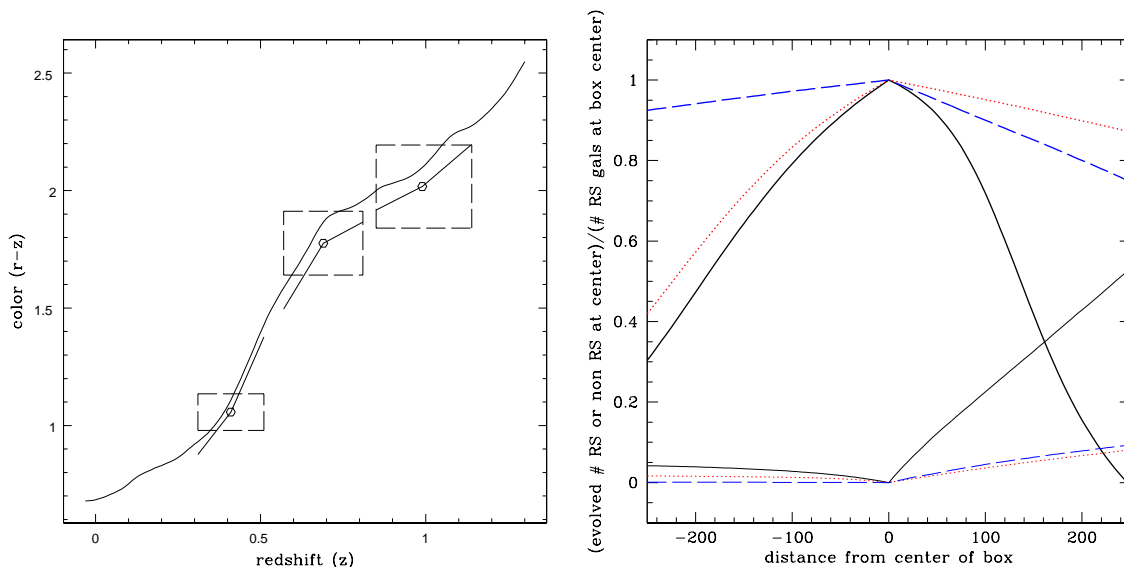


**Figure 2.** **a)** Solid lines show the  $r-z$  color evolution of a  $z = 3$  burst population synthesis model of Bruzual & Charlot (2003). Circles show the mean colors of MS red sequence galaxies at the three redshifts we investigate, while straight line segments give the color gradients applied when projecting the galaxy population along a line-of-sight (Table 1). Vertical portions of the dashed boxes at each epoch mark the foreground and background redshifts of the  $\pm 250 h^{-1}$  Mpc volume, while the horizontal lines mark the approximate width of the red sequence. **b)** The relative fraction of galaxies remaining on the red sequence as a function of projected distance (heavy lines). Solid, dotted, and dashed lines correspond to  $z = 0.41, 0.69$  and  $0.99$ , respectively. Thin lines give the relative number of galaxies that move onto the red sequence as their observed color and magnitude vary due to their line-of-sight displacement. All counts are normalized by the number of red sequence galaxies within the volume at each redshift.

considered  $i$  band, our results for this case are described at the end of §4; results below will be given for  $r-z$  unless stated otherwise.

## 2.1 Galaxy Colors in Massive Halos

Fig. 1 shows that a red sequence in  $r-z$  vs.  $z$  exists in rich MS halos over the range of redshifts probed. We use galaxies above  $\sim \frac{1}{2}L_*$ , corresponding to  $z$ -magnitudes of 19.6, 21 and 22 at redshifts 0.41, 0.69 and 0.99, and yielding samples of 942313, 1005469 and 1054711 galaxies, respectively. The top panels show contours of the full, magnitude-limited population while lower panels show the color-magnitude behavior of galaxies in halos with 8 or more members.

Taking galaxies within the inner  $0.5 h^{-1}$  Mpc of the centers of the latter sample, we fit a linear relation in the  $r-z$  vs.  $z$  plane. Following Gladders et al (1998), we throw out  $3\sigma$  outliers and iterate the fit to find the slope and intercept of the red sequence. The width of the red sequence is set to enclose 90% of the full massive halo galaxy sample. The distance,  $\Delta_{\perp}$ , is taken perpendicular to the red sequence line in the color-magnitude space.<sup>8</sup> Table 1 lists the slopes, intercepts, and widths of the red sequence for all three redshifts. The red sequence color-magnitude relation is a weak

<sup>8</sup> If one instead uses  $> 90\%$  of these galaxies, the red sequence widens and for high redshift slightly increases the contamination from projection under study here.

function of halo mass or richness, so the parameters are not particularly sensitive to the choice of halos with 8 or more members.

Defining the red sequence using the MS galaxy population itself means that our color cuts are optimally tuned to the content of the MS massive halos. With observations, one derives color cuts using the color-magnitude data of a target subset of galaxies, such as the approaches used by Gladders et al (1998) and Koester et al (2007). Comparing the simulation results to observations, it appears that the mock red sequence has the wrong tilt and is slightly wider than observed. We experimented with “tightening” the red sequence by moving the galaxy colors closer to the best-fit line, but such a procedure did not have a large effect on our conclusions so we present our results using colors as provided.

We wish to use projections of each proper time output to create finite redshift segments of a full sky survey. Starting with the coeval MS galaxy samples, we introduce passive color and magnitude evolution into spatial projections to mimic the behavior of a light-cone population. The color evolution with redshift is based on an instantaneous Bruzual-Charlot (BC) burst at  $z \approx 3$  and shown for  $r - z$  in Fig. 2a.<sup>9</sup> For comparison, we show the average (slightly bluer) color of the MS red sequence galaxies for our three redshifts. The MS red sequence galaxies are expected to be bluer than the BC model, since their stars were not formed in a single burst at high redshift. The MS galaxies are also bluer than BCG’s in the SDSS (Bernardi et al 2007).

We use this simple BC model to define piecewise constant color gradients,  $d(r - z)/d\text{redshift}$ , along the line of sight, shown by the solid line segments in Fig.2a. We define a  $z$  magnitude gradient analogously. Foreground and background color-magnitude evolution are modeled separately, with parameters given in Table 1. Fainter galaxies may evolve into the  $z$  magnitude cut because of the change in observed magnitude with redshift. To catch these potential interlopers, we employ galaxy catalogues half a magnitude fainter in  $z$ -band than required by the unevolved red sequence cuts.

Note that the applied color gradient becomes progressively shallower at higher redshift. The assumed degree of color and magnitude evolution is key since it controls the redshift filtering power of the red sequence. To foreshadow one of our main results, Fig. 2a illustrates how the color evolution determines the line-of-sight path length probed by the red sequence color range. The dashed regions in Fig. 2a are centered at the average color of the red sequence galaxies at each redshift and are bounded vertically by the approximate range of color of the red sequence. They are bounded horizontally by the redshift extents of the comoving  $\pm 250 h^{-1}$  Mpc sightline available within the MS volume. At  $z = 0.41$ , the evolutionary color gradients are strong enough that projected red sequence galaxies will shift out of the target color range before the  $\pm 250 h^{-1}$  Mpc MS boundary is reached, but this is not quite the case at  $z = 0.69$  and 0.99.

<sup>9</sup> We thank N. Padmanabhan and B. Koester for the evolution of galaxy colors using Bruzual & Charlot (2003) as in Padmanabhan et al (2006).

Fig.2b further illustrates how the imposed color evolution acts as a redshift filter. Taking the color and magnitude of each galaxy and our line of sight gradients, Fig.2b shows the fraction of these galaxies remaining on the red sequence as a function of line-of-sight distance. Such galaxies will still be potential members of a cluster centered at the origin. A more narrowly peaked distribution indicates a smaller fraction of galaxies available for inclusion via projection during cluster finding. As can be seen, the fraction of galaxies remaining within the red sequence cut at large distances from the origin increases with redshift; the red sequence selects a longer path along line of sight at higher redshift.

The other source of contamination is galaxies that are shifted into the red sequence by the change in observed color. The number density of these galaxies, normalized by the number of red sequence galaxies at the central redshift, is shown by the light lines in Fig.2b. Except for the most distant part of the box at  $z = 0.41$ , this number is relatively small. Our use of a uniform color change with redshift for all galaxies is not strictly correct for all galaxy types. However, blue star forming galaxies change in observed color much more slowly with redshift than in this model, so to be shifted erroneously into our red sequence color cut, these galaxies are required to be at significantly higher redshift than the cluster. Since they would then lie outside of our  $500 h^{-1}$  Mpc box, they are not included in our analysis. The strongest contribution to interloper candidates is from galaxies which have colors within our red sequence color cut even though they are far from the central galaxy along the line of sight.

## 2.2 Cluster Finding Algorithm

Our algorithm defines clusters as circular regions, centered on a bright galaxy, with red-sequence sky surface density equal to a multiple  $\Delta_p$  of the mean value at the redshift of interest. This approach is analogous to the spherical overdensity method used to define the halo masses. For target centers, we work in descending order through a list of red-sequence galaxies ranked (brightest to dimmest) by apparent  $z$ -band magnitude. This ranking is motivated by a desire to find the rare, high mass halos first, then work down the mass function to more common objects.

Around a potential cluster center, a radially-sorted list of red sequence neighbors is used to define a mean galaxy number density profile as a function of transverse separation. We use the periodic boundaries of the MS to recenter the simulated volume on each candidate center. The volume extends  $250 h^{-1}$  Mpc in front and behind, and galaxy colors are adjusted, linearly with distance in the projected direction, as described above. Starting with the 8 nearest neighbors, (to avoid shot noise problems in tracing the cluster profiles at small radii), we work outward in radius  $r_{\text{gal}}$  until the the number of galaxies  $N_{\text{gal}}$  fails to satisfy the overdensity criterion

$$\Delta \equiv \frac{N_{\text{gal}}}{\bar{n}\pi r_{\text{gal}}^2} \geq \Delta_p. \quad (1)$$

Here  $\bar{n}$  is the mean sky surface density of red sequence galaxies in the MS, including the effects of the applied observed color evolution along the projected dimension. If the overdensity criterion is not satisfied for 8 galaxies, the object is

discarded, if  $N_{\text{gal}}$  meets or exceeds a minimum of 8 galaxies, then this cluster is added to the output list. All members are then recorded and removed from the remaining list of potential cluster centers.<sup>10</sup>

Note that area overlap of clusters is allowed, so that a single galaxy can belong to more than one cluster (6-7% of the galaxies end up in more than one cluster at the lowest 2 redshifts, dropping to 4–5% at higher redshifts; in contrast, galaxies only belong to one MS halo). To boost statistics, we make three projections of the simulated volume along its principal axes.

The choice of  $\Delta_p$  is discussed below. The sensitivity of survey purity and completeness to the choice of  $\Delta_p$  is further explored in the appendix.

### 2.3 Cluster–Halo Matching

The clusters found by the search algorithm can be linked back to the dark matter halos in the simulation using their respective lists of galaxy members. A perfect algorithm would be complete with respect to halos and have no false positives, *i.e.*, no clusters that appear rich on the sky but are actually several less rich systems aligned along the line-of-sight. In addition, the halo and cluster richnesses would agree. A perfect algorithm would therefore recover the intrinsic distribution of halo mass  $M$  as a function of red sequence galaxy richness  $N_{\text{gal}}$ . This distribution is shown in the top panels of Fig. 3.

At all redshifts, a mean, red sequence richness of  $N_{\text{gal}} \simeq 20$  above our  $z$ -magnitude limit corresponds to a  $\sim 10^{14} h^{-1} M_{\odot}$  halo. When fit (throwing out 3- $\sigma$  outliers several times) above a minimum of 8 members, we find that mass scales with red sequence richness as  $M=M_{20}(N_{\text{gal}}-1)^{\alpha}$ , with  $\alpha = 1.07, 1.10$  and  $1.10$  at  $z=0.41, 0.69$  and  $0.99$  respectively. The mass intercepts are  $M_{20}=1.3, 1.3$  and  $1.5 \times 10^{14} h^{-1} M_{\odot}$  and there are  $\sim 4100, 2900,$  and  $1300$   $N_{\text{gal}} \geq 8$  halos at these redshifts, respectively. Note that red sequence richness is a fairly noisy tracer of mass; the rms level of scatter is  $\sim 50\%$  or higher above the richness cut of  $N_{\text{gal}}=8$  (a detailed discussion of scatter in richness vs. mass can be found in White & Kochanek (2002); Dai, Kochanek & Morgan (2007)). The richness we use in finding the clusters may not be the best richness to use for getting the cluster mass (e.g. galaxy counts within some aperture might be useful after the clusters are found, for finding the clusters themselves we found a fixed aperture performed significantly worse). Some observational surveys for galaxy overdensities account for projections of foreground/background galaxies via a statistical subtraction of the expected number of projected galaxies, calculated from

<sup>10</sup> Roughly the cluster will have a density of red sequence galaxies  $\Delta_p$  times the average red sequence (background) density,  $\sim 0.7/(h^{-1} \text{Mpc})^2$  in our case. The approximate change of radius with richness can be read off from Eq.1. Note too that our cluster-finding algorithm traces galaxy overdensities to radii which can potentially reach greater than  $1 h^{-1} \text{Mpc}$ . This algorithm increases the survey sensitivity to truly extended structures, but may also increase the cross-section for interlopers relative to algorithms which search for clusters only on a limited, smaller scale; however, a fixed aperture richness based cluster finder performed significantly more poorly.

random non-cluster pointings. Our cluster richness estimator,  $N_{\text{gal}}$ , does not include such a correction; our overdensity requirement means that approximately  $1/\Delta_p$  of the galaxies are from the background.

For each cluster identified in projection, we list all halos contributing one or more of its member galaxies. The quality of the cluster detection is measured by the top-ranked matched fraction,  $f_{1h}$ , defined as the fraction of cluster members coming from the halo that contributes the plurality of the cluster’s red sequence galaxies. We define two classes, *clean* and *blended*, based on whether the plurality is or is not the majority of the cluster’s membership,

$$\text{clean} \quad : \quad f_{1h} \geq 0.5, \quad (2)$$

$$\text{blended} \quad : \quad f_{1h} < 0.5, \quad (3)$$

We assign to each cluster the mass of its top-ranked halo found through member-matching. If two (or more) halos contribute the same number of galaxies, and are both top-ranked, we take the most massive.

## 3 RESULTS

An ideal cluster catalog would be *pure*, *complete* and *unbiased* with respect to halos. A perfectly *pure* sample would have no accidental projections; all the galaxies of any chosen cluster would be common members of a single, dark matter halo. A perfectly *complete* sample would be one for which each halo in the survey volume appears once, and only once, in the list of clusters. Finally, an *unbiased* cluster catalog would contain clusters that reproduce the mean mass-richness relation defined by halos. In this section, we consider these issues, both in the context of setting our circular overdensity threshold and in the results obtained. We will see that high levels of purity and completeness are achieved, and that the cluster samples are nearly unbiased. (Many definitions of purity and completeness exist in the literature, we describe and compare several of them in the appendix, and detail our definitions as we use them below.)

### 3.1 Cluster finder threshold and two examples

The cluster catalogs produced by the search algorithm depend on the value of the number density threshold  $\Delta_p$ . Choosing too high a value will pick out only the cores of the richest halos, resulting in a catalog that is pure and complete at very high masses, but is otherwise incomplete. Picking too low a value will extend the search into the periphery of halos, leading to a catalog that, although complete across a wide range of masses, suffers from impurities due to blending multiple halos into a single cluster.

Our choice of  $\Delta_p = 7$  and  $N_{\text{obs}} \geq 8$  for clusters provides samples that are highly complete for  $N_{\text{true}} \geq 20$  halos. Fig. 4 shows a measure of completeness, the fraction of halos assigned as top-ranked matches to clusters with  $N_{\text{gal}} \geq 8$ . The completeness is very high for halos with intrinsic  $N_{\text{true}} \geq 20$ , but it drops considerably for lower-richness halos. More halos are missed at higher redshift, and these tend to have extended, filamentary shapes suggestive of recent (or imminent) merging. At higher redshift, the major merger rate increases, leading to a higher fraction of disturbed halos.

Keeping the cluster richness fixed at  $N_{\text{obs}} \geq 8$  in order

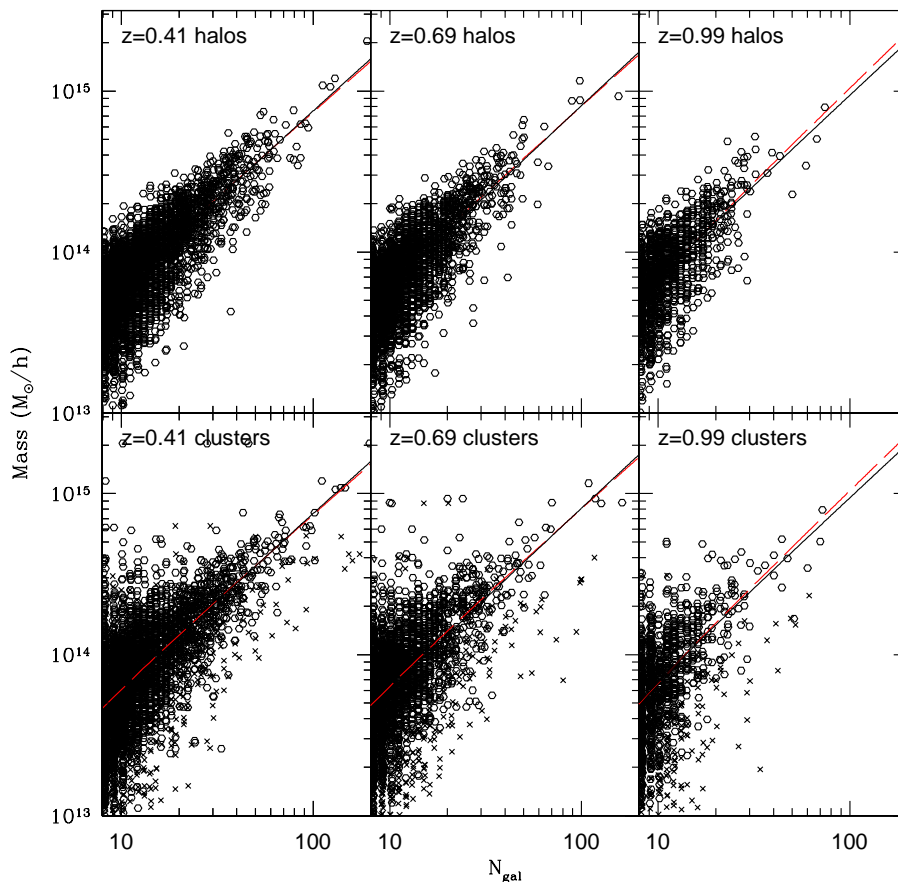


**Figure 3.** Top: Relation between halo mass and intrinsic red sequence galaxy richness at  $z=0.41, 0.69$ , and  $0.99$  (left to right). Bottom: Relation between top-ranked halo mass and cluster red sequence galaxy richness at the same redshifts, taken along one projection axis. Crosses have  $f_{1h} < 0.5$  and comprise (12%, 15%, 20%) of the  $N_{\text{gal}} \geq 8$  clusters. Solid (dashed) lines are least-squares fits for  $N_{\text{gal}} \geq 8$  halos (clean clusters).

to define whether a halo is found or not (completeness), samples derived with higher values of  $\Delta_p$  will be more pure (have fewer blends) but less complete, and vice-versa for samples constructed with lower  $\Delta_p$ . Further quantitative discussion on purity and completeness can be found in the appendix.

Fig.5 shows that, at each redshift, the value  $\Delta_p = 7$  produces a cluster catalog with a richness function,  $n(N_{\text{gal}})$ , that matches well that of the underlying halo population. Averaging the three projections, there are 4432, 2919 and 1321 clusters with  $N_{\text{gal}} \geq 8$  at  $z = 0.41, 0.69$  and  $0.99$ , respectively. These values compare well to the MS halo counts of 4098, 2926, 1290 for  $N_{\text{gal}} \geq 8$ . The scatter from the average of cluster numbers between different lines of sight is less than a percent at  $z = 0.41$  and less than four percent at  $z = 0.99$ .

The good match in number counts does not imply that the algorithm is perfect. In fact, the typical number of halos contributing to an  $N_{\text{gal}} \geq 8$  cluster is  $\sim N_{\text{gal}}/4$ . The second and fifth richest clusters found at  $z = 0.41$  illustrate the range of behavior in clean and blended clusters. Figure 6 shows projected positions and color-magnitude information for sky patches centered on the two clusters. The second

richest cluster has 212 members contributed by 21 different halos. Members of one of the most massive halos at that epoch,  $M = 2.0 \times 10^{15} h^{-1} M_{\odot}$ , comprise 88% of the cluster members. The remaining members come from 20 other halos, including some lying in the foreground. A small number of members are contributed by halos in the background.

The fifth richest cluster, with 175 members, presents a very different case. Its most massive contributing halo has a mass  $M = 4.2 \times 10^{14} h^{-1} M_{\odot}$ , which contributes almost all of its own galaxies but only 35% of the cluster's members ( $f_{1h} = 0.35$ ). A total of 53 other halos also contribute, many lying close (within  $\lesssim 30 h^{-1}$  Mpc) in the foreground or background.

Although much richer than most of the halos considered, these two examples illustrate the essential projection problem that is causing the blends; both sets of galaxies appear to be reasonable clusters in the x-y plane. In the next two sections the statistics of the clean and blended clusters, and their features, will be discussed in more detail.

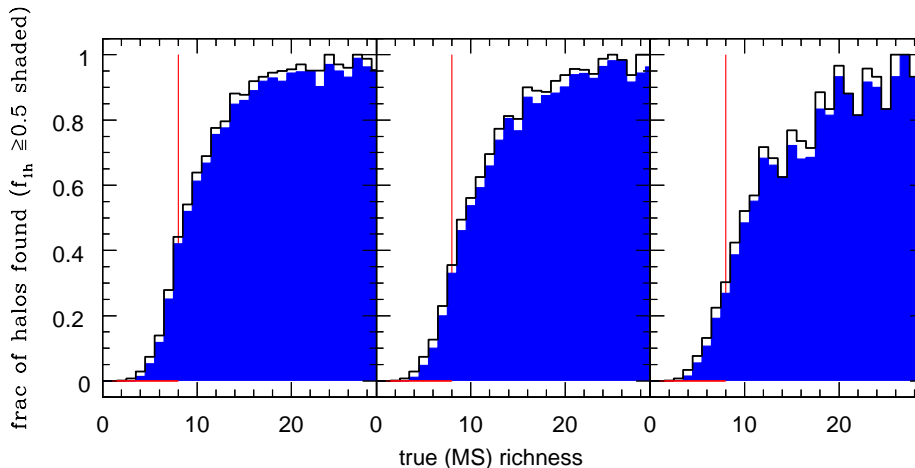


**Figure 4.** Differential completeness of the  $N_{\text{obs}} \geq 8$  cluster population with respect to halos as a function of their intrinsic red-sequence richness. The circular overdensity defining the cluster population is  $\Delta_p = 7$  and panels show results for (left to right) redshifts  $z = 0.41, 0.69, 0.99$ . Here, completeness is the fraction of halos that contribute the plurality of a cluster’s red sequence galaxy population. The solid line is the fraction associated with all clusters and the shaded region is fraction found in clean ( $f_{1h} \geq 0.5$ ) clusters. The vertical line is the minimum imposed cluster richness imposed ( $N_{\text{min}} = 8$ ). Projection effects introduce scatter between intrinsic and apparent richness that blurs the sharp observed threshold into a smooth intrinsic selection function.

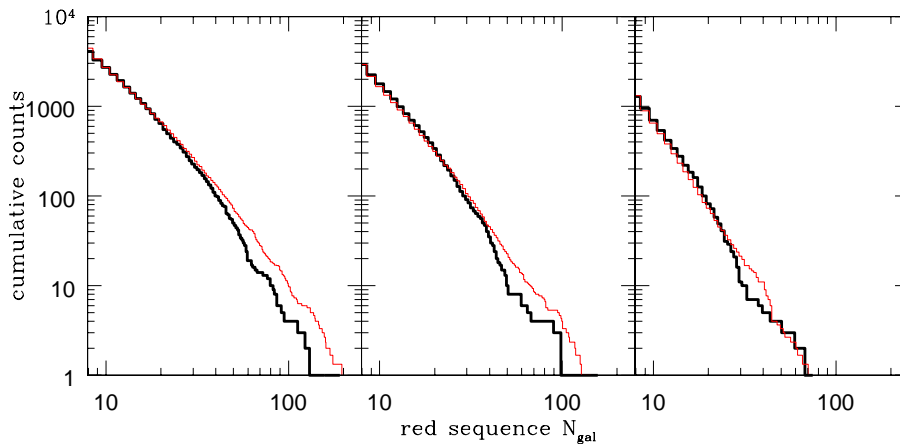


**Figure 5.** Cumulative number of halos as a function of red sequence richness  $N_{\text{gal}}$  (bold) compared to the projection-averaged number of clusters found with the circular overdensity algorithm with  $\Delta_p = 7$  (light) at redshifts  $z = 0.41, 0.69$  and  $0.99$  (left to right).

### 3.2 Mass selection function of clusters

The mass selection function is an important ingredient for cosmological tests with optical cluster surveys (White & Kochanek (2002), Rozo et al (2007)). Fig. 3 (bottom) shows the relationship between the observed richness of a cluster and the mass of its top-ranked halo (see § 2.3). Circles show clean clusters while small crosses show blends. At each redshift, the clean cluster population displays a power law mean relation remarkably similar to that of the underlying halo population. The slopes of the relations agree at

the few percent level; the values for halos (clean clusters) for  $N_{\text{gal}} \geq 8$  are 1.07 (1.04), 1.10 (1.06), 1.10 (1.15) from low to high redshift, respectively. The intercepts at  $N_{\text{gal}} = 20$  also agree at the few percent level, and could be further fine-tuned by introducing small changes to the search threshold  $\Delta_p$  at each redshift. At all redshifts, the circular overdensity algorithm is effective at identifying the mean richness-mass behavior of the underlying halo population.

The dispersion in the observed cluster sample is larger than for halos, due to failure modes of the search algo-

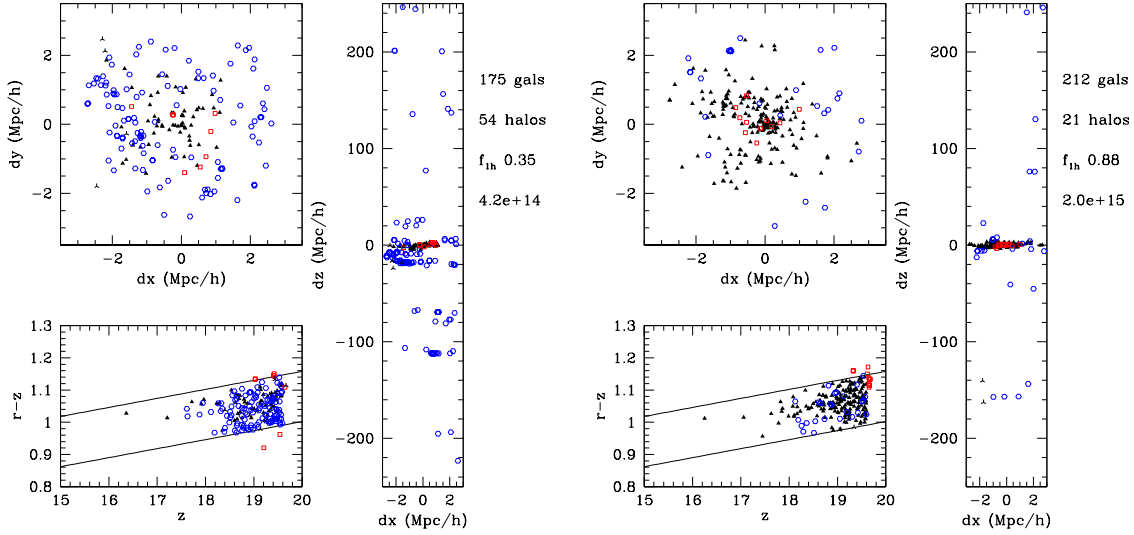


**Figure 6.** Examples of blended (left, 5th richest) and clean (right, 2nd richest) clusters found at  $z=0.41$ . Filled triangles are members of the first-rank matched halo, open circles are other cluster members. Open squares are members of the best fit halo not in the cluster; they fall outside the red sequence as can be seen in the lower left hand panel. Triangular stars are members of the red sequence not in the found cluster. Comoving scales are shown, note that the axes in the  $dz$  vs.  $dx$  figure are scaled differently.

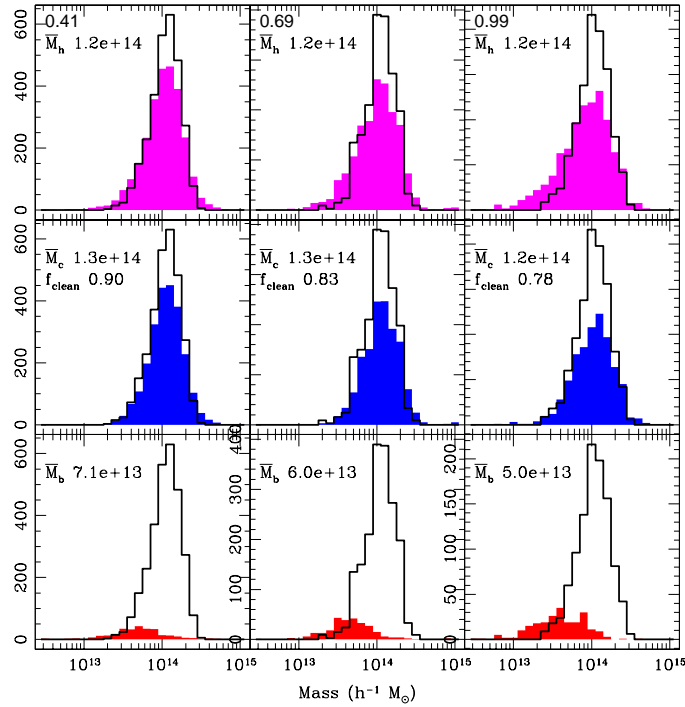


**Figure 7.** Mass selection functions  $p(M|N_{\text{gal}}, z)$  with richness  $N_{\text{gal}} = (18, 18, 16) \pm 4$  at redshifts  $z = (0.41, 0.69, 0.99)$  (left to right). Solid lines give the intrinsic halo mass distribution in these richness ranges, and are the same in each column. The shaded distribution in the upper row gives  $p(M|N_{\text{gal}})$  for clusters, with  $M$  the mass of its top-ranked matched halo (§ 2.3). The middle row shows  $p(M|N_{\text{gal}})$  for clean clusters ( $f_{1h} \geq 0.5$ ) while the bottom row gives the mass distribution of blended clusters ( $f_{1h} < 0.5$ ). The average mass of the halos/clean clusters/blended clusters are shown respectively in the top/middle/bottom panels for each redshift. The fraction of clean clusters  $f_{\text{clean}}$  is also given in the middle row for each redshift.



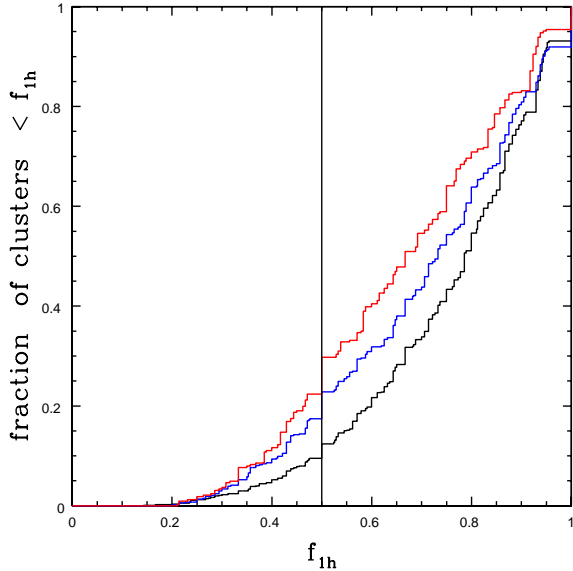


**Figure 8.** Cumulative fraction of clusters in Fig. 7 as a function of their top-ranked halo overlap fraction,  $f_{1h}$ . Top to bottom lines are redshifts,  $z=0.99$ ,  $0.69$  and  $0.41$ . The fraction of galaxies from the top-ranked halo declines with increasing redshift. The vertical line identifies the fraction of clusters that are blends,  $f_{1h} < 0.5$ .

At fixed observed richness, blending creates a tail to low masses while fragmentation of large halos into multiple clusters introduces a high mass tail. Fig. 7 shows estimates of the conditional halo mass distribution,  $p(M|N_{\text{gal}}, z)$ , derived from cross-sections of the joint likelihood data in Fig. 3 in richness ranges  $N_{\text{gal}} = (18, 18, 16) \pm 4$  at redshifts  $(0.41, 0.69, 0.99)$ , respectively. This choice gives a constant average halo mass,  $1.2 \times 10^{14} h^{-1} M_{\odot}$ , at all three redshifts.

The cluster likelihoods (shaded in the figure) are compared with the halo distributions for the same richness ranges, shown by solid lines. The top row shows all clusters, while the middle and bottom rows separate the samples into clean and blended systems, respectively. Raw counts rather than normalized likelihoods are shown to give the number of objects.

At  $z=0.41$ , more than 90% of clusters in the chosen richness range have their dominant underlying halo contributing at least half of the galaxies. The mass distribution of the found clusters matches well the underlying halo mass likelihood. At higher redshift, the correspondence between halos and clusters weakens somewhat; the number of blends more than doubles, from  $< 10\%$  at  $z=0.41$  to  $22\%$  at  $z=0.99$ . The blended systems contribute a low mass tail to the halo mass likelihood. For the distributions, the central mass of the clean clusters remains at  $1.2 - 1.3 \times 10^{14} h^{-1} M_{\odot}$  at all 3 redshifts, while the central mass of the blends drops, from  $7.1 \times 10^{13} h^{-1} M_{\odot}$  at  $z = 0.41$  to  $5.0 \times 10^{13} h^{-1} M_{\odot}$ . Thus the ratio of central masses between the clean and blended clusters also increases with redshift.

Our classification of clean versus blended clusters is based on a somewhat arbitrary cutoff of 0.5 in member fraction. Figure 8 provides a more complete picture by plotting the cumulative fraction of clusters that have top-ranked halo member fraction  $< f_{1h}$ . Here the same observed cluster rich-

ness limits as in Fig. 7 are used. Cutting at  $f_{1h} \geq 0.5$ , the vertical line, gives the clean fractions quoted in Fig. 7. Analogues for other definitions of “clean fraction” in terms of  $f_{1h}$  can be read off as well. There is a clear trend with redshift, with clusters at  $z=0.99$  being less well-matched to halos than those at  $z=0.41$ . The median value of  $f_{1h}$  tells a similar story, decreasing from  $\sim 0.8$  at  $z=0.41$  to  $\sim 0.7$  at  $z=0.99$ . Blending is clearly increasing at larger redshift.

Going to a higher central mass gives similar trends, e.g. centering on a richness corresponding to a average  $1.5 \times 10^{14} h^{-1} M_{\odot}$  halo mass at all redshifts gives a clean fraction of 90% at redshift 0.41 which decreases to 76% at redshift 0.99 for the same  $\Delta_p$  as above ( $\Delta_p$  can be increased for higher richness to improve both numbers but the increase of blends at high redshift remains).

### 3.3 Causes and trends for blends

There are several effects which cause an increasing incidence of blends at higher redshift. Firstly, the change of observed color with distance is weaker, and secondly, the red sequence is wider, so the color-magnitude cut selects galaxies from a thicker slice along the line of sight. These seem to be the strongest causes and were illustrated in Fig. 2.

Another way of seeing the effect of color/magnitude evolution is to remove it entirely at  $z = 0.41$ ; the background level then increases and the contrast between the clusters and the background declines. Lowering  $\Delta_p$  to obtain the same number of clean clusters at the fixed mass range of Fig. 7, we find that the level of blends increases to  $\sim 20\%$ , very close to what is seen at  $z \sim 0.99$ . Similarly, to increase the clean fraction, one can impose the  $z = 0.41$  color evolution on the  $z = 0.99$  population. In this case, however, the number of non-red sequence galaxies brought into the red sequence through our evolution increases strongly, limiting the degree to which blends can be reduced.

A third contributing factor is that, at earlier times, the mass function is steeper, causing the number of possible interloper halos per target halo (of mass  $\sim 10^{14} h^{-1} M_{\odot}$ , for example) to grow at high redshift. The increase in intermediate-mass halos is also enhanced because the central galaxy magnitude is less well correlated with host halo mass at  $z=0.99$  than at low redshift. Over time, central galaxies in massive halos grow and brighten via mergers, leading to a stronger correlation between  $z$ -magnitude and halo mass. Our cluster finding algorithm works in descending order of luminosity. At low redshift, the luminosity sorting corresponds well to a sorting in halo mass but, at high redshift, more low mass systems are mixed into the range of central galaxy magnitude occupied by high mass halos.

As these factors are fairly generic, as expected, the trend toward more blends at  $z=0.99$  appeared in all the cases we considered: changing definition and tightness of the red sequence, changing  $N_{\text{gal}}$  cuts and changing the spherical overdensity requirement. For a wide range of density cuts and modeling choices the blends have roughly half the mass of the clean matches at  $z = 0.41$ , and this mass scale declines at higher redshift.

**Table 2.** Expected Cluster X-ray Properties.

Redshift	$\langle L \rangle_{\text{halo}}^a$	$\langle L \rangle_{\text{clean}}^a$	$\langle L \rangle_{\text{blends}}^a$	$f_{\text{blends}}$
0.41	1.4 (0.96)	1.6 (1.0)	0.84 (1.5)	0.11
0.69	1.4 (0.96)	1.8 (1.1)	0.70 (1.3)	0.16
0.99	1.8 (0.97)	2.0 (1.1)	0.56 (1.3)	0.23

<sup>a</sup> Numbers in parenthesis give the log-normal scatter,  $\sigma_{\ln L}$ .

#### 4 IMPLICATIONS

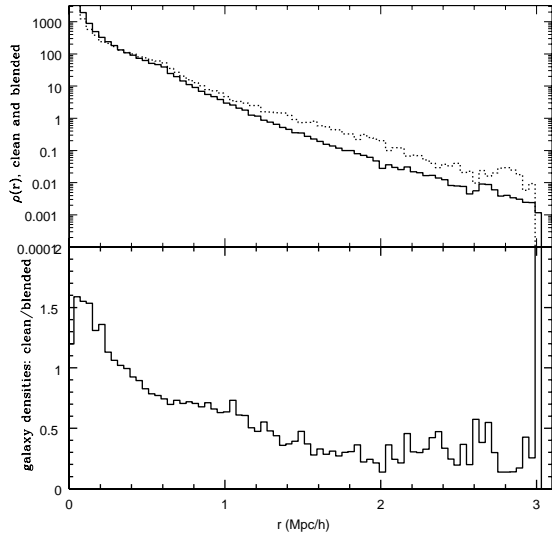
Since blended clusters are associated with lower mass halos, they will be evident in follow-up studies as such. Their mean lensing signal, X-ray luminosity and temperature, and thermal SZ decrement should be low relative to clean systems. Spectroscopic signatures of substructure, in the form of multiple peaks or other departures from Gaussianity, would also be likely in these systems. The imprecise centering of the multiple components along the line-of-sight would tend to flatten the radial number density profile.

Table 2 provides estimates of the soft band X-ray luminosity from our MS blended and clean clusters with richness  $18 \pm 4$  (now fixed across redshifts), compared to values for halos of the same richness. We assume a power-law relation of the form  $L \propto (M/10^{14} h^{-1} M_{\odot})^{1.6}$  (Staneke et al 2006), and quote values normalized, arbitrarily, to the luminosity of a  $10^{14} h^{-1} M_{\odot}$  halo at each epoch. We also assume scatter in the mass-luminosity relation,  $\sigma_{\ln M} = 0.4$ , and combine this with the dispersion in mass for the chosen richness range (Fig.7) to give the dispersion in luminosity,  $\sigma_{\ln L}$ . Lower values have been suggested for  $\sigma_{\ln M}$  (Reiprich & Boehringer 2002), but the scatter in mass at fixed  $N_{\text{gal}}$  dominates the intrinsic L-M scatter anyway.

The clean clusters have mean X-ray luminosities that tend to be slightly higher than the corresponding values for halos of the same richness. The blended systems are substantially dimmer, by a factor two in the mean at  $z = 0.41$ , growing to a factor three at  $z = 0.99$ .

Blends should be a generic outcome of red sequence-based cluster finding methods, and there are indications of this from initial X-ray and dynamical observations of the RCS clusters. In Chandra observations of 13 clusters at  $0.6 < z < 1.0$ , Hicks et al (2005, 2007) confirm 12 as X-ray sources at  $3-\sigma$  significance, suggesting that  $> 90\%$  of the cluster candidates are massive structures with deep gravitational potential wells (see also Blindert et al (2007)). However, their X-ray luminosities were systematically lower at a given cluster richness than seen for lower-redshift X-ray selected clusters. Most of the clusters lay on a sequence only slightly offset from the expected  $L_x$ -richness relation, but several clusters were significantly offset. Optical spectroscopy of one of these clusters (at  $z = 0.9$ ) showed that it consisted of several structures which are dynamically discrete but whose red sequences were overlapping in the survey data (Gilbank et al 2007)– precisely the sort of blended system expected by the study here (see also van Breukelen et al (2007)). Evidence for large scatter between X-ray luminosity and optical richness has been seen in e.g. Yee & Ellingson (2003); Gilbank et al (2004); Lubin, Mulchaey & Postman (2004); Hicks et al (2005); Barkhouse et al (2006).

Instead of using only the top-ranked halo mass to determine the X-ray signal, we can instead sum the luminosity of



**Figure 9.** “Stacked” profiles of clusters with  $f_{1h} \geq 0.5$  divided by those with  $f_{1h} < 0.5$  for the  $\Delta_p = 7.0$  case and  $z = 0.41$ . The case here is representative, the trend of ratio with radius was seen in all redshifts and color cuts. Stacking after rescaling by the outer radius gave similar results.

all contributing halos. In this case, all the cluster luminosities go up, with the clean subset increasing by roughly 0.3 and the blended subset increasing by a larger amount. Then the ratio of clean to blended mean luminosities changes to  $\sim 1.2$  at low redshift and to  $\sim 2.4$  at high redshift. The luminosity measured by X-ray observation will depend on details of the projected spatial arrangement, the noise characteristics and other details that lie beyond the scope of this investigation. It seems reasonable to consider the values quoted for the single halo case as a lower bound, and the values from summing all halos as an upper bound, on what would be observed.

Another difference between clean and blended systems is in their radial cluster profiles. Stacked profiles of the clean and blended clusters are used to produce the density profiles,  $\rho(r) = \frac{1}{N_{\text{clus}}} N(r)/(r^2 dr)$ , shown in Fig. 9. The clean clusters have a significantly steeper mean density profile than the blends. This result suggests that a matched angular filter approach (Postman et al 1996) could offer improvements, particularly one that includes radial distance information from photometric redshifts or colors (White & Kochanek 2002). Observations of colors with distance to cluster center (e.g. Ellingson et al (2001); Blindert et al. (2004)) and other properties (e.g. De Lucia et al (2004)) are already in place at high redshifts. Going further down the luminosity function would provide more galaxies to trace out the profile, but at the risk of including more faint background galaxies redshifted into the color region.

The interlopers in both clean and blended clusters, as expected by Gladders & Yee (2000), lie (slightly) more frequently in the background than the foreground. There doesn’t seem to be a strong trend in the moment of inertia for clean versus blended clusters; often the blends are projections, rather than objects which are merely unrelaxed.

We also considered using  $i - z$  color at high redshift,

rather than  $r - z$ , and found a similar blend fraction, even though the red sequence turns out to be narrower. This is because the evolution of red sequence galaxies (now defined with respect to  $i - z$ ) remains very slow with redshift, thus, as with  $r - z$  color at high redshift, many of the galaxies do not evolve out of the red sequence even when far from the cluster center. Similarly, the number of non-red sequence galaxies evolving into the selection window remains small across the  $\pm 250 h^{-1}$  Gpc projected length.

As mentioned earlier, blends can be immediately reduced by increasing the spherical overdensity criterion  $\Delta_p$ , but only at the cost of losing true halos as well. An increase in  $\Delta_p$  also shifts the mass-richness relation to lower values of  $N_{\text{gal}}$  compared to the intrinsic case, and decreases the number of clusters found at fixed  $N_{\text{gal}}$ . These trends reflect the usual tradeoff between purity and completeness for cluster samples; for more discussion see, e.g., the appendix of White & Kochanek (2002) and the appendix of this paper.

## 5 DISCUSSION

In the above analysis, we have found properties and trends for blends as a function of redshift. Some of these results depend on particular details of the Millennium Simulation and our method, and some are likely to be general.

Most of the increase in blends at  $z \sim 1$  comes from the slower change of color with increasing redshift. This color change was not obtained directly from the Millennium simulation but from a simple stellar population synthesis model that reproduces observations. We expect this result to be general. Our implementation of the color change with redshift is crude but the candidate high redshift interlopers are mostly red sequence galaxies, where our approximation is best expected to hold. As a result, we do not expect more detailed color implementations, such as mock light cones (e.g. Kitzbichler and White (2007) for the MS), to produce substantially different local ( $\pm 100 h^{-1}$  Mpc) projected contamination.

The increased width of the red sequence at high redshift is derived from the Millennium Simulation. However, at  $z=0.99$ , the weak color evolution combined with the deep “green valley” separating the red and blue populations in the MS means that our results are reasonably insensitive to the precise width. Most of the interloper galaxies are themselves members of the red sequence in their respective projected halos. The  $r - z$  color shift for  $\pm 250 h^{-1}$  Mpc projection at  $z = 0.99$  is  $-0.1$  and  $+0.18$ , so only by compressing the red sequence to a width well below these values would one have an appreciable effect on the blended fraction.

The relative numbers of interloper halos at different redshifts is a property of the underlying dark matter power spectrum and linear growth rate. For a fixed target mass, more interloper halos at higher redshift are expected generically. Physically, if we look at the line-of-sight distribution of the contaminating material we find that the contaminating mass at large distances ( $> 50 h^{-1}$  Mpc) more than doubles between redshift 0.41 and 0.99. This enhanced contamination from large distances is also true on a cluster-by-cluster basis: the fraction of clusters with more than e.g. 30% of their material coming from  $> 40 h^{-1}$  Mpc grows significantly with redshift. This material is far outside the cluster virial

radius and not just material which got “caught” by the cluster finder before it fell in to truly be part of the cluster. Note that superclusters of very large size have been seen out at these redshifts, for example see recent studies of superclusters by Gal, Lubin & Squires (2005); Nakata et al (2005).

There are other possible interlopers as well. For instance, adding galaxies that lie outside the MS volume will only increase the amount of blended contamination. Also, at faint magnitudes, the increasing numbers of background blue galaxies available to redshift into the red sequence are a potential cause for concern; increasing numbers of blue galaxies at high redshift are observed (e.g. Ellis (1997)). (It should be noted that there are observational techniques to take many of them out which we do not include here). We saw only a small fraction of candidate interlopers from galaxies outside the red sequence, except at low redshift, where the green valley is highly compressed (see Fig.2). This is good, as the observed color and magnitude evolution of these galaxies was approximated to be the same as for red sequence galaxies; we expect the interloper numbers due to these objects is minimized at high redshift because of their small contribution in our approximation. In fact, taking out the observed color and magnitude evolution of the non-red-sequence galaxies entirely (and adjusting  $\Delta_p$  to get the same value of  $\bar{n}\Delta_p$ ) gives similar clean fractions as in our fiducial model.

To extend our analysis of the MS (tuning the cluster finder to cluster color profiles in more detail, for example) requires further developments. The MS utilizes sophisticated physical models for properties such as star formation histories, initial mass function and stellar population synthesis models, dust production and radiative transfer models, and the sensitivity of all of these to local conditions. The resulting MS catalogues match observations of large numbers of properties (e.g. Springel et al (2005); Lemson et al (2006); Croton et al (2006); Kitzbichler and White (2007)) at many redshifts. A detailed, multi-color comparison to observed galaxy number counts is given in Kitzbichler and White (2007). Some departures from observations are noted there, in particular the over-prediction of the abundance of moderately massive galaxies at high redshifts, notably  $z > 1$ .

For our cluster finding, the only properties used are the galaxy locations and their fluxes in two filters. Tuning the cluster finder to more specific properties of these fluxes (for example, their radial trends within clusters) in the MS will require higher fidelity galaxy formation models. Work is in progress to improve the model’s match to observations. For example, known issues in the MS under study include, for  $z = 0$  clusters, a faint red satellite excess and an excess tail of bright blue objects (but with overall blue satellite fractions too low), and no “green valley” (Weinmann et al 2006a; De Lucia 2006; De Lucia et al 2007). We find a red sequence with the wrong sign for the color-magnitude slope (the brightest galaxies tend to be slightly bluer than the fainter, see Fig. 1), and similarly the blue fraction increases towards brighter luminosity and has the wrong radial evolution within clusters for our three redshifts. In addition the simulation was run with the earlier WMAP parameters rather than the WMAP3 (Spergel et al 2006) current best fit cosmology.

Future improvements in optical cluster finding will require simulated catalogues that are in better quantitative

agreement with the growing body of deep galaxy surveys. To refine and use more sophisticated color finders does not necessarily require all the physics employed in the MS, which aims to explain a multitude of observational properties rather than simply reproduce them. Purely statistical mock catalogues can be built on halo model fits tuned empirically to data in the redshift range of interest. The catalogues can focus narrowly on observational properties relevant to the search algorithm. In particular, critical to a quantitative prediction of the amount of contamination in color-selected surveys are accurate colors for galaxies in groups and filaments in the outskirts of clusters, as red-sequence galaxies in these regions are the most likely source of interlopers.

Such survey-specific catalogues are crucial to understand selection functions, in part because they allowing search algorithms to be tuned to the cluster “color footprint” and spatial profile. This approach has already been profitably used at low redshifts (e.g. Kochanek et al 2003; Eke et al 2004; Yan, White & Coil 2004; Yang et al 2005; Miller et al 2005; Weinmann et al 2006b; Miller et al 2005; Koester et al 2007). At high redshift, data sets large enough to tune such catalogues are just coming into being; combined with modeling improvements in recent years the construction of such catalogues is now a feasible task.

However, without such a catalogue in hand, our primary effect is still simple to illustrate. This effect is that the spatial cut provided by the observed color and magnitude cut widens as redshift increases. Conversely a narrow spatial cut reduces the blends strongly. For example, taking an exact spatial cut for the MS, boxes  $100 h^{-1} \text{Mpc}$  wide at all three redshifts, the clean fraction becomes almost 100% at low redshift and 95% at high redshift. (Presumably the remaining blends are due to the other contributing factors mentioned above.) A slice this thick would correspond to a fine redshift selection,  $\Delta z = 0.06(0.04)$  at redshift 0.99 (0.41). This level of accuracy is potentially attainable with next-generation photometric redshifts.

## 6 CONCLUSIONS

With the advent of wide field imagers, optical searches have become a powerful way to compile large samples of high redshift clusters. Key to these techniques is the use of multi-color information to reduce the line-of-sight contamination that plagued earlier, single filter, observations (Abell 1958; Dalton et al 1992; Lumsden et al 1992; White et al 1999). Two-filter information provides only limited redshift filtering, and this paper begins to explore the questions of what types of objects are selected by such techniques, and how this selection evolves with redshift.

We use a simple circular overdensity search algorithm on local sky projections of the galaxy population of the Millennium Simulation, tuned using knowledge of the red sequence present in simulated halos with eight or more galaxies brighter than  $L_*/2$  in the  $z$ -band. The free parameter, the density contrast  $\Delta_p$ , is tuned to maximize both purity and completeness, and the choice  $\Delta_p = 7$  produces a number of clusters as a function of galaxy richness that is close to the underlying richness function of halos.

We find that essentially all clusters have some degree of projected contamination; a cluster of optical richness  $N_{\text{gal}}$

typically has red sequence members from  $N_{\text{gal}}/4$  halos along the line-of-sight. In the large majority of cases, the contamination is not dominant, and most of a cluster’s members are associated with a single, massive halo. A minority are highly blended cases in which projected contamination is dominant, and no single halo contributes a majority of the cluster’s members.

We find an increased fraction of blends with redshift. Although several factors contribute, the most important factor appears to be weaker evolution in the observed color of red sequence galaxies with increasing redshift. This effectively increases the path length searched by the red sequence color cut, leading to a larger cross section for accidental, line-of-sight projections. In addition, at higher redshift, the number of  $\sim 3 \times 10^{13} h^{-1} M_{\odot}$  halos relative to a  $10^{14} h^{-1} M_{\odot}$  halo is larger, and the central galaxy red magnitudes at these mass scales are more similar.

The blends add a low-mass tail to the halo mass selection function for clusters of fixed optical richness. For our found clusters with optical richness targeting  $10^{14} h^{-1} M_{\odot}$  halos, we expect that  $\sim 10\%$  of these systems would be underluminous in X-rays by a factor of two at  $z = 0.41$ , growing to  $\sim 20\%$  underluminous by a factor closer to three at  $z = 0.99$ . The scatter in individual X-ray luminosities for the complete set of clusters is expected to be large,  $\sigma_{\ln L} \simeq 1.2$  at high redshift, and there is considerable overlap in the distributions of  $L_X$  expected for clean and blended clusters. It should be noted that, observationally, high redshift low-luminosity systems are also likely have lower signal to noise.

The galaxy number density profiles are slightly shallower for blends than for clean clusters, and a matched spatial filter approach may help identify and eliminate the former. Since some fraction of halos, those undergoing mergers especially, will also be spatially extended, careful study of the effect of spatial filtering on halo completeness is needed. Alternatively, instead of decreasing the number of blends in searches, our findings here suggest modeling the mass likelihood  $p(M|N_{\text{gal}}, z)$  as a bimodal log-normal distribution, with the fraction of blends, and the location and width of that component, included as nuisance parameters. This expected bimodal distribution can be incorporated into error estimates for cluster number counts as a function of redshift, for instance, along with other expected errors (such as the 5-10% scatter associated with red sequence associated redshifts Gilbank et al 2007).

Understanding the detailed color/magnitude trends within galaxy clusters is key to refining red sequence cluster finding and improving its success rate. Fortunately, data sets in hand or on the way, combined with rapidly improving modeling methods, will lead to improvements in our understanding of high redshift colors and their evolution. This work will be driven largely by survey-specific mocks—current examples are the 2MASS (Kochanek et al 2003), the DEEP2 survey (Yan, White & Coil 2004), the 2dFGRS (Eke et al 2004; Yang et al 2005) and the SDSS (Miller et al 2005; Koester et al 2007; Weinmann et al 2006b) — and such efforts will be necessary for mining the rich science provided by existing and future high redshift cluster surveys.

We thank the anonymous referee for many helpful comments and suggestions. JDC thanks A. Albrecht, M. Brod-

win, C. Fassnacht, R. Gal, J. Hennawi, A. von der Linden, L. Lubin, G. De Lucia, S. Majumdar, T. McKay, N. Padmanabhan, E. Rozo, R. Stanek and D. Weinberg for helpful discussions and/or questions and the Galileo Galilei Institute, the Santa Fe Cosmology Summer Workshop, and the Aspen Center for Physics for hospitality during the course of this work and the opportunity to present these results, and LBL for support. AEE thanks J. Annis and T. McKay for conversations and acknowledges support from NASA grant NAG5-13378, from NSF ITR ACI-0121671, and especially from the Miller Institute for Basic Research in Science at UC, Berkeley. MW thanks Charles Lawrence for conversations. DJC wishes to thank both the Aspen Center for Physics and the Department of Physics at the University of Michigan for hospitality, and acknowledge support from NSF grant AST507428. MW acknowledges support from NASA and EE acknowledges support from NSF grant AST-0206154. The Millennium Simulation was carried out by the Virgo Supercomputing Consortium at the Computing Centre of the Max-Planck Society in Garching; semi-analytic galaxy catalogues are publicly available at <http://www.mpa-garching.mpg.de/Millennium/>.

## APPENDIX

Purity and completeness are “success rates” used when one wants a catalogue of a certain type of object and has obtained, via some method, a catalogue of candidates. A classic definition starts with the number of objects which are both in the candidate set and in the desired target set, i.e. the intersection of these sets. Dividing the number in the intersection by the total number of target objects then gives completeness, and dividing by the total number of candidate objects gives purity (or reliability). These definitions go back many years in radio astronomy. For instance Condon, Balonek & Jauncey (1975) used these definitions to describe how well optical sources were matched to radio sources as a function of search aperture radius. In our case, target objects are halos, defined in terms of true richness or mass, and candidate objects are clusters, defined in terms of observed richness.

While these terms have a long history, it is not clear that such definitions are the ‘single number’ one wants to characterize the success of a cluster finding algorithm. If the properties of the sample change slowly with e.g. richness or mass for example, we may not wish to impose a hard threshold on richness when computing purity. Finding a cluster with 19 members may be just as good as requiring 20. We shall consider several generalizations of the classic notions of purity and completeness below.

We note that there are several choices in all of these definitions: the two catalogues, including their underlying data samples and the search algorithms employed, and the definition of which clusters lie in the intersection. Even focussing on the circular overdensity method, as we do here, there is considerable latitude in defining both the target catalogue (e.g., specific definition of a halo, use of halo richness or mass as the order parameter) and the cluster candidate sample (minimum observed cluster richness, choice of  $\Delta_p$ ). We consider here how purity and completeness vary with  $\Delta_p$ .

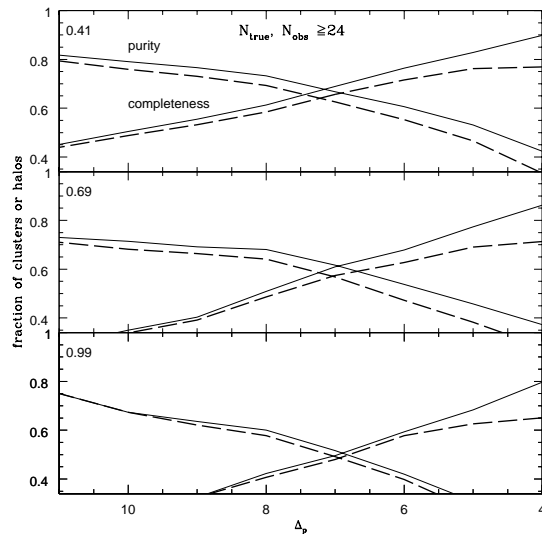


**Figure 10.** Purity and completeness as a function of overdensity contrast  $\Delta_p$  in Eq. 1 for  $z = 0.41, 0.69, 0.99$ , top to bottom. The target catalogue is halos with  $24 \leq N_{\text{true}} \leq 100$  and the candidate clusters have  $24 \leq N_{\text{obs}}$ . The number of objects in the overlap of the two catalogues is divided by the total number of objects in the target halo catalogue to get completeness (rising lines) and by the total number of objects in the candidate cluster catalogue to get purity (falling lines). The overlap of the two catalogues is either taken to be either target halos which contribute the most galaxies to a candidate cluster (solid line) or only target halos which contribute at least half of their cluster galaxies (dashed line), i.e. only halos that match to clean clusters.

Figure 10 shows the classic definitions of purity and completeness applied to our catalogues for target halos with true richness  $24 \leq N_{\text{true}} \leq 100$  and candidate clusters with observed richness  $\geq 24$ . We define a cluster and its halo to be in the overlap of the two catalogues if the halo in the target set contributes the most galaxies to a cluster in the candidate set. A more restrictive definition is to require the halo to contribute more than half of the galaxies in a given cluster ( $f_{1h} \geq 0.5$ ). In both cases, one divides the overlap number by the total number of target halos (completeness) and total number of candidate clusters (purity). In Fig. 10, these two cases (all  $f_{1h}$  and  $f_{1h} \geq 0.5$ ) for the overlap set are shown as smooth and dashed lines, respectively.

We show Fig. 10 as a function of *decreasing* overdensity threshold,  $\Delta_p$ , because this mimics a search region of increasing radial scale. At high  $\Delta_p$ , purity is maximized because the cluster sample is selecting the dense cores of the most massive halos. As the threshold is decreased, the enlarged search area and lower intrinsic density within the halo increases the frequency of best matched halos which are below the target richness threshold, lowering the cluster sample purity. In contrast, the completeness grows with lower  $\Delta_p$ , as the increasing search scale matches and then exceeds the radial scale used to define the halo population. The number of observed clusters at fixed richness increases rapidly with decreasing  $\Delta_p$ , improving the odds of completely matching to the massive halo sample. The purity and completeness curves cross at roughly our chosen threshold,  $\Delta_p \simeq 7$ .

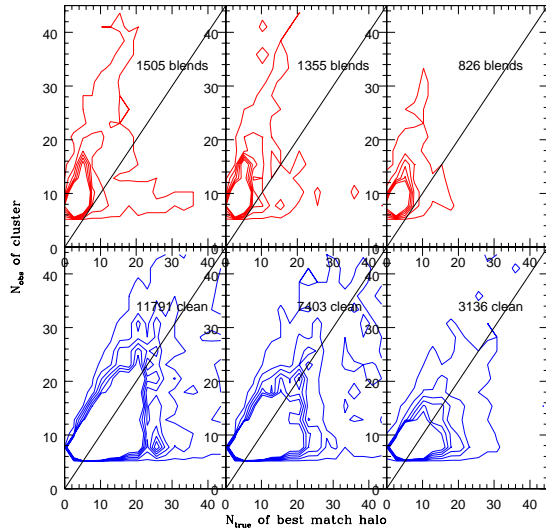


**Figure 11.** Scatter between true halo richness (x-axis) and observed cluster richness (y-axis), for blends (top) and clean clusters (bottom), for  $z = 0.41, 0.69, 0.99$  (left to right) summed over all three projection axes. Even for the clean clusters the scatter is extremely large. Contours differ by 10, starting at 2, and the pixel size is 2.5. The straight line is  $N_{\text{true}} = N_{\text{obs}}$ .

These measures of purity and completeness are substantially lower than unity because, as shown in Fig.11, there is substantial scatter between  $N_{\text{true}}$  and  $N_{\text{obs}}$  for matched halo-cluster pairs. This should not be taken as a failure of the algorithm, because the source of impurity and incompleteness – the scatter – is largely understood. There are a number of ways to take this scatter into account, and the optimal method depends strongly on the intended use of the catalogue. Different target/candidate sets will vary in purity and completeness, driven by the form of the scatter. To characterize this one could, for example, use  $N_{\text{true}} \geq N$ ,  $N_{\text{obs}} \geq N - \delta$  to calculate completeness, and  $N_{\text{true}} \geq N - \delta$ ,  $N_{\text{obs}} \geq N$  to calculate purity. If one approximates the scatter as Poisson an obvious choice for  $N = 25$  would be  $\delta = \sqrt{N} \simeq 5$ . For  $N = 24$  using  $\delta = 5$  raises the fractions for completeness and purity by  $\sim 0.1 - 0.2$  (the largest change is at  $\Delta_p$  for low completeness or purity, the smallest at high completeness or purity), while using  $\delta = 10$  roughly doubles the effect. The purity and completeness curves still cross around  $\Delta_p \simeq 7$  (slightly lower for  $z = 0.41$ ) but at a higher fraction (for  $z = 0.41$  it goes from  $\sim 0.7$  to  $\sim 0.85$  to  $\sim 0.95$  for shifts by 5 and 10, respectively). Note that the *a priori* arbitrary choice of  $\delta$  should be motivated by some understanding of how the sample properties change with the property being used to define the sample.

Extending the candidate sample when defining completeness and the target sample when defining purity can be taken further. We can take the target halo  $N_{\text{true}}$  above some cut and consider *all* clusters above the minimum richness threshold (which could be as low as one) to define completeness, for example. In our case the minimum richness threshold is  $N_{\text{obs}} \geq 8$ . The differential form of completeness for  $N_{\text{obs}} \geq 8$  and  $\Delta_p = 7$  is shown in Fig. 4 in the main text. For purity one can again reverse the limits. If one goes to

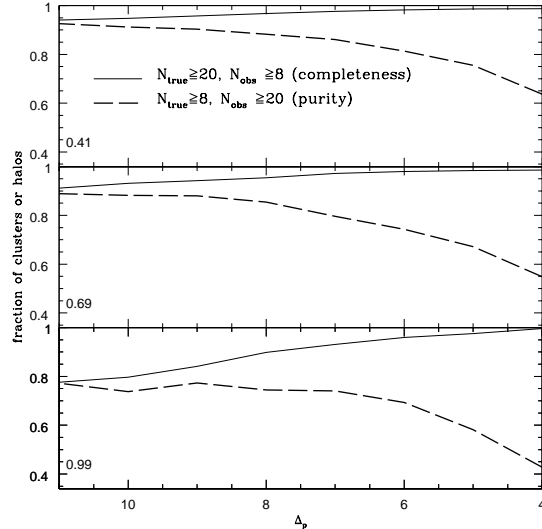


**Figure 12.** Purity and completeness as a function of overdensity contrast  $\Delta_p$  for  $z = 0.41, 0.69, 0.99$ , top to bottom. Unlike Fig. 10, the target and candidate samples used to define purity and completeness differ. For completeness (increasing line), the target catalogue is halos with  $20 \leq N_{\text{true}} \leq 100$  and the candidate clusters are any found cluster (i.e.  $8 \leq N_{\text{obs}}$ ), both clean and blended. For purity (decreasing line), the candidate catalogue comprises all clusters with  $N_{\text{obs}} \geq 20$ , the target set is halos with  $8 \leq N_{\text{true}} \leq 100$ , and a halo is only taken to be in the intersection if it contributes the majority of galaxies to a cluster, i.e. this purity is simply the fraction of clean clusters,  $f_{\text{clean}}$ . Completeness decreases and purity increases with increasing  $\Delta_p$ .

$N_{\text{true}} \geq 1$ , all clusters will get matched to at least one halo, and values close to this will have similar results. A possibly more useful definition of purity could be that the best matched halo contributes at least 0.5 of its partner cluster's members. This definition of purity corresponds to the clean fraction shown in Fig. 7.

Fig. 12 shows the purity and completeness for these less restrictive sample definitions, taking  $N = 20$  and  $\delta = 12$ . The solid increasing line and the dashed decreasing line (with decreasing  $\Delta_p$ ) are directly analogous to their counterparts in Fig. 10. At high surface density  $\Delta_p$ , the  $N_{\text{obs}} \geq 8$  cluster sample is incomplete with respect to  $100 \geq N_{\text{true}} \geq 20$  halos because the cores of some  $N_{\text{true}} \geq 20$  halos fall below the cluster richness limit of 8 members. As mentioned in the text, high redshift high mass halos are more likely to be disturbed than their lower redshift counterparts and thus to fall below the overdensity threshold. The purity of the overall cluster sample purity is very high at  $z = 0.4$ , but declines at higher redshift where halo blending is more severe.

As the threshold  $\Delta_p$  is lowered, the fraction of halo galaxies lying above the projected threshold increases, but the potential for confusion by projection also increases. For  $\Delta_p = 4$ , the  $N_{\text{obs}} \geq 8$  cluster sample is essentially 100% complete for  $N_{\text{true}} \geq 20$  halos at all redshifts. The overall purity of the  $N_{\text{obs}} \geq 20$  cluster sample is substantially lower, dropping to values below 0.5 at  $z = 1$ .

Another way of choosing the two samples is pursued by

Rozo et al (2007), who take Fig. 11, combining both blends and clean clusters, and identify strong outliers (see their Fig. 2). They take a slice in a fixed  $N_{\text{obs}}$  range to define purity (number which are not outliers over total in slice) and a slice in a fixed  $N_{\text{true}}$  range to define completeness (number which are not outliers over total in slice). The issue of how outliers are defined and which slices in  $N_{\text{obs}}$ ,  $N_{\text{true}}$  are taken will affect the detailed results, and, again, the intended use of the catalogue needs to be taken into account before deciding the optimal choices.

The difficulty in finding the best definition lies in trying to get two numbers (purity and completeness) to characterize an entire joint distribution. The full distribution of candidate properties as a function of target halo properties is the key information required to compute expectations for an observational catalogue. The scatter is not a problem if its shape is sufficiently well understood and the required accuracy for understanding this distribution depends upon the specific use of the catalogue. For instance, high purity (but not necessarily high completeness) might be of interest if one is interested in high mass clusters for individual X-ray followup, while if one wants a sample of clusters for cosmological parameters, a scatter in mass can be included in the analysis, but high completeness is desirable to beat down statistics. If one can correct for scatter perfectly, obtaining high purity is then not crucial; purity serves only to quantify the size of the correction being applied to the data or the model. The errors that are most important to avoid, and how well characterized our selection function is, determines the best line of attack in the tradeoff between purity and completeness.

## REFERENCES

- Abell, G.O., 1958, ApJS 3,211  
 Barkhouse, W.A., et al, 2006, ApJ, 645, 955  
 Bernardi, M., Hyde, J.B., Sheth, R.K., Miller, C.J., Nichol, R.C., 2007, AJ 133, 1741  
 Blindert, K., Yee, H. K. C., Gladders, M. D., & Ellingson, E. 2004, IAU Colloq. 195: Outskirts of Galaxy Clusters: Intense Life in the Suburbs, 215  
 Blindert et al, 2007, to appear  
 Bower, R., Lucey, J.R., & Ellis, R.S., 1992, MNRAS, 254, 601  
 Bruzual, G., Charlot, S., 2003, MNRAS 344, 1000  
 Condon, J. J., Balonek, T.J., Jauncey, D.L., 1975, AJ, 80, 887  
 Croton et al, 2006, MNRAS 365, 11  
 Dai, X., Kochanek, C.S., Morgan, N.D., 2007, ApJ 658, 917  
 Dalton, G.B., Efstathiou, G., Maddox, S.J., & Sutherland, W.J., 1992, ApJL 390, L1  
 Davis M., Efstathiou G., Frenk C.S., White S.D.M., 1985, ApJ, 292, 371  
 De Lucia, G., et al, 2004, ApJL 610, 7  
 De Lucia, G., to appear, talk at Berkeley Nov. 2006  
 De Lucia, G., et al, 2007, MNRAS 374, 809  
 Eke, V.R., et al, 2004, MNRAS 348, 866  
 Ellingson, E., Lin, H., Yee, H.K.C., Carlberg, R.G., 2001, ApJ 547, 609  
 Ellis, R.S., 1997, ARA&A 35, 389  
 Gal, R. R., Lubin, L. M., Squires, G. K., 2005, AJ, 129, 1827  
 Gal, R.R., 2006, preprint [astro-ph/0601195]  
 Gilbank, D.G., Bower, R.G., Castander, F.J., Ziegler, B.L., 2004, MNRAS 348, 551  
 Gilbank, D.G., Yee, H.K.C., Ellingson, E., Gladders, M.D., Barrientos, L.F., Blindert, K., 2007, ApJ in press, preprint [arxiv/0705.0782]  
 Gladders, M.D., Lopez-Cruz, O., Yee, H.K.C., Kodama, T., 1998, ApJ 501, 571  
 Gladders, M.D., Yee, H.K.C., 2000, AJ 120, 2148, see also <http://www.astro.utoronto.ca/~gladders/RCS/>  
 Gladders, M.D., Yee, H.K.C., 2005, ApJS 157, 1  
 Gladders, M.D., et al, 2007, ApJ 655, 128  
 Hicks, A., Ellingson, E., Bautz, M., Yee, H., Gladders, M., 2005, AdSpR 36, 706  
 Hicks, A., et al, 2007, to appear  
 Kaiser, N., Wilson, G., Luppino, G., Kofman, L., Gioia, I. Metzger, M., Dahle, H., 1998, preprint [astro-ph/9809268]  
 Kitzbichler, M.G., White, S.D.M., 2007, MNRAS 376, 2  
 Kochanek, C.S., White, M., Huchra, J., Macri, L., Jarrett, T.H., Schneider, S.E., Mader, J., 2003, ApJ 585, 161  
 Koester B.P., McKay, T.A., et al, 2007, preprint [astro-ph/0701268]  
 Lemson, G. & the Virgo Consortium, 2006, preprint [astro-ph/0608019]  
 Lopez-Cruz, O., 1997, PhD thesis, University of Toronto  
 Lopez-Cruz, O., Barkhouse, W.A., Yee, H.K.C., 2004, ApJ 614, 679  
 Lubin, L.M., Brunner, R., Metzger, M.R., Postman, M., Oke, J.B., 2000, ApJL, 531, 5  
 Lubin, L.M., Mulchaey, J.S., Postman, M., 2004, ApJL 601, 9  
 Lumsden, S.L., Nichol, R.C., Collins, C.A., Guzzo, L., 1992, MNRAS 258,1  
 Miller, C.J., et al, 2005, AJ 130, 968  
 Nakata, F., et al, 2005, MNRAS 357, 1357  
 Padmanabhan, N., et al, 2006, preprint [astro-ph/0605302]  
 Postman, M., Lubin, L.M., Gunn, J.E., Oke, J.B., Hoessel, J.G., Schneider, D.P., Christensen, J.A., 1996, AJ 111, 615  
 Reblinsky, K., & Bartelmann, M., 1999, A & A 345,1  
 Reiprich, T.H., Boehringer, H., 2002, ApJ 567, 716  
 Rozo, E., Wechsler, R.H., Koester, B.P., Evrard, A.E., McKay, T.A., 2007, preprint [astro-ph/0703574]  
 Spergel et al, 2006, preprint [astro-ph/0603449]  
 Springel, V., et al, 2005, Nature 435, 629  
 Stanek, R., Evrard, A.E., Boehringer, H., Schuecker, P., Nord, B., 2006, ApJ 648, 956  
 van Breukelen, C., et al., 2007, preprint [arXiv:0708.3838]  
 van Haarlem, M.P., Frenk, C.S., White, S.D.M., 1997, MNRAS, 287, 817  
 Weinmann, S.M., van den Bosch, F.C. Yang, X., Mo, H.J., 2006a, astro-ph/0607585, to appear in the proceedings of the XLII Rencontres de Moriond, XXVth Astrophysics Moriond Meeting: "From dark halos to light", Eds. L.Tresse, S. Maurogordato and J. Tran Thanh Van (Editions Frontieres)  
 Weinmann, S.M., van den Bosch, F.C., Yang, X., Mo, H.J., 2006b, MNRAS 373, 1159  
 White, R., et al 1999, AJ 118, 2014  
 White, M., A&A 367 (2001) 27

- White, M., Kochanek, C.S., 2002, ApJ 574, 24  
Wilson, G., 2006, preprint [astro-ph/0604289],  
<http://spider.ipac.caltech.edu/staff/gillian/SpARCS>  
Yan, R., White, M., Coil, A.L., 2004, ApJ 607, 739  
Yang X., Mo H.J., van den Bosch F.C., Jing Y.P., 2005,  
MNRAS, 356, 1293  
Yee, H.K.C., Ellingson, E., 2003, Apj 585, 215